

Panchromatic All-Polymer Photodetector with Tunable Polarization Sensitivity

Pratik Sen, Ruonan Yang, Jeromy J. Rech, Yuanxiang Feng, Carr Hoi Yi Ho, Jinsong Huang, Franky So, R. Joseph Kline, Wei You, Michael W. Kudenov, and Brendan T. O'Connor*

In this report, a high-performance all-polymer organic photodetector that is sensitive to linearly polarized light throughout the visible spectrum is demonstrated. The active layer is a bulk heterojunction composed of an electron donor polymer PBnDT-FTAZ and acceptor polymer P(NDI2OD-T2) that have complementary spectral absorption resulting in efficient detection from 350 to 800 nm. The blend film exhibits good ductility with the ability to accommodate large strains of over 60% without fracture. This allows the film to undergo large uniaxial strain resulting in in-plane alignment of both polymers making the film optically anisotropic and intrinsically polarization sensitive. The films are characterized by UV-vis spectroscopy and grazing incidence wide-angle X-ray scattering showing that both polymers have similar in-plane backbone alignment and maintain packing order after being strained. The films are integrated into devices and characterized under linear polarized light. The strain-oriented detectors have maximum photocurrent anisotropies of 1.4 under transverse polarized light while maintaining peak responsivities of 0.21 A W^{-1} and a 3 dB cutoff frequency of $\approx 1 \text{ kHz}$. The demonstrated performance is comparable to the current state of the art all-polymer photodetectors with the added capability of polarization sensitivity enabling new application opportunities.

intensity over a specific wavelength range. However, in addition to intensity and wavelength, the polarization state is a primary characteristic of electromagnetic radiation. Determining the polarization state adds significant information about the light being detected that is beneficial for a range of applications including remote sensing, environmental monitoring, telecommunication, astronomy, and chemical/biomedical sensing.^[1,2] Currently, the most common photodetectors are based on silicon,^[3] and polarization sensitivity is achieved by employing a wire-grid polarizer on the input side of the photodiode. This approach is effective but can reject a significant portion of the incident light. It also increases the detector's complexity. An attractive alternative is to employ intrinsic polarization-sensitive active layers in the device. One promising material system with this capability is polymer semiconductors. Polymer-based photodetectors have been of growing research interest due to their compatibility with low-temperature processing onto a variety

1. Introduction

The primary objective of photodetectors is to sense electromagnetic radiation and convert the signal into an electrical output. In most cases, photodetectors focus on capturing light

of substrates, flexibility, low-weight, and their ability to tune spectral sensitivity through molecular design.^[4–7] In addition to their spectral tunability, a less exploited feature is their ability to achieve intrinsic polarization sensitivity.^[8–11] This feature can be exploited to achieve photodetectors that are polarization sensitive

P. Sen, Prof. B. T. O'Connor
Department of Mechanical and Aerospace Engineering
North Carolina State University
Raleigh, NC 27695, USA
E-mail: btoconno@ncsu.edu


R. Yang, Prof. M. W. Kudenov
Department of Electrical and Computer Engineering
North Carolina State University
Raleigh, NC 27695, USA

J. J. Rech, Prof. W. You
Department of Chemistry
University of North Carolina
Chapel Hill, NC 27599, USA

Y. Feng, Prof. J. Huang
Department of Applied Physical Sciences
University of North Carolina
Chapel Hill, NC 27599, USA

Dr. C. H. Y. Ho, Prof. F. So
Department of Materials Science and Engineering
North Carolina State University
Raleigh, NC 27695, USA

Dr. R. J. Kline
Materials Science and Engineering Division
National Institute of Standards and Technology
Gaithersburg, MD 20899, USA

 The ORCID identification number(s) for the author(s) of this article can be found under <https://doi.org/10.1002/adom.201801346>.

DOI: 10.1002/adom.201801346

without the need of additional light-manipulating optics. This reduced complexity simplifies polarization-sensitive devices,^[12–17] and opens up new opportunities in detector architectures such as polarized detectors in tandem to realize compact coincident polarimeters (polarization state detectors).^[15,16]

Most polymer semiconductors have their primary optical transition dipole moment (π - π^*) aligned along their backbone.^[10,18] Thus, orienting the polymer backbone in a film results in anisotropic optical and electrical properties.^[8,11] This unique property of polymer semiconductors has been exploited to achieve polarized light-emitting diodes and polarized photovoltaics.^[9,12–16] There have been numerous processes to achieve oriented films that include alignment during solution processing,^[19–21] or post solidification film manipulation.^[12–16] One common approach is to apply an external mechanical load to a cast film by physically rubbing or uniaxial stretching.^[12–16] An advantage of these two techniques is the ability to tune the magnitude of polymer alignment that in turn dictates polarization sensitivity, which is important in optimizing the performance of polarimeters.^[15,16] Although rubbing has been demonstrated to produce films with significant diattenuation, the method can lead to uneven surfaces that may result in devices prone to shorting.^[13,22,23] Alternatively, uniaxially straining the films is a well-controlled method for polymer alignment, where the induced anisotropy is controlled by the extent of applied strain. Strain aligning the active semiconductor layer has been successfully used to fabricate polarization-sensitive detectors.^[15,16] However, to date, polarization-sensitive organic photodetectors have only been fabricated with the polymer poly(3-hexylthiophene) (P3HT) and small molecule phenyl-C₆₁butyric acid methyl ester (PCBM).^[14–16] Due to the poor absorption of PCBM in the visible spectrum, the spectral

sensitivity of the detector was largely defined by P3HT and limited to light below ≈ 625 nm.

To achieve polarized detectors with panchromatic sensitivity, replacing the fullerene electron acceptor is desired. Recently, there have been a number of small molecule acceptors developed to replace fullerenes in organic photovoltaics enabling broad spectral sensitivity.^[24–26] However, achieving oriented small molecules within the bulk heterojunction (BHJ) to induce polarization sensitivity of both semiconductor components is extremely difficult to realize. Furthermore, most small molecules act as antiplasticizers, resulting in polymer:small molecule blend films being relatively brittle. This prevents the ability to strain orient the film to achieve significant polarization sensitivity.^[27,28] An alternative is to employ polymer semiconductors for both the electron donor and acceptor in the BHJ, where strain alignment would result in both polymers becoming sensitive to polarized light. Recent reports have highlighted that all-polymer photovoltaic blends can be more ductile than similar polymer:small molecule systems.^[29,30] The performance of all-polymer photovoltaics have also been improving recently with the development of new donor-acceptor copolymers.^[31,32] However, the focus of all-polymer photovoltaics has largely been on solar power, and there have been limited reports of all-polymer photodiodes, due primarily to the relatively nascent state of the field.^[33–38]

In this report, we present an all-polymer photodetector system capable of polarization sensitivity from the near-UV to the near-IR. The polarization-sensitive active layer is a BHJ composing of the electron donor PBnDT-FTAZ and the electron acceptor P(NDI2OD-T2), also known as N2200.^[39,40] The chemical structure of these two materials is depicted in **Figure 1a**. We show that the blend film can be strain-oriented, as illustrated in **Figure 1c**, resulting in broad tuning of the device polarization sensitivity. The morphology of the films

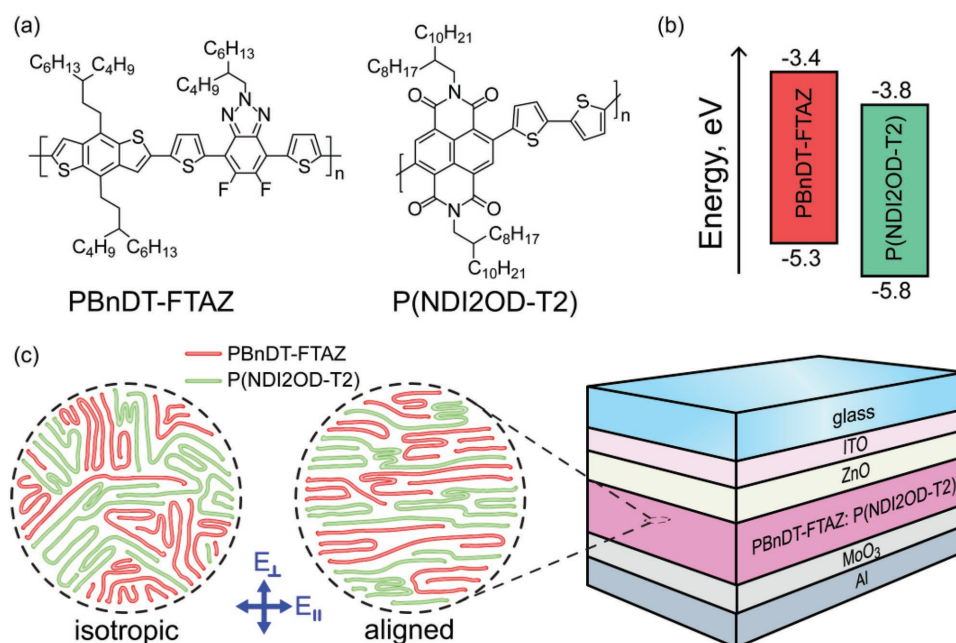


Figure 1. a) Chemical structure of PBnDT-FTAZ and P(NDI2OD-T2). b) HOMO and LUMO energy levels for PBnDT-FTAZ and P(NDI2OD-T2). c) Top-view schematic of polymer chain organization in the case of spun-cast isotropic film and a strain-oriented polarization-sensitive film. Schematic includes relative orientation of the polarized light field (L and $||$) used throughout this article. Right, the organic photodetector device stack.

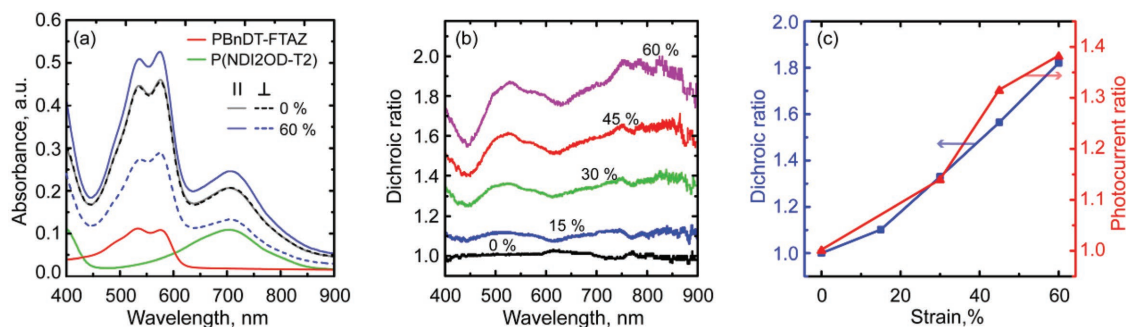


Figure 2. a) Absorbance spectra of PBnDT-FTAZ:P(NDI2OD-T2) blend films under linear polarized light parallel (||) and perpendicular (⊥) to the direction of applied strain. Measurements are given for a spun-cast (0%) and 60% strained film. The absorbance of neat polymer films are also provided to show the contribution of each material to the total absorbance. b) The dichroic ratio spectra of the blend films with applied strain. c) The dichroic ratio of the blend films at 575 nm with applied strain, and the photocurrent anisotropy of the detectors measured under linear polarized white light (AM1.5G solar spectrum). The photocurrent was measured at a bias of -0.5 V.

was characterized by UV-vis spectroscopy, grazing incidence wide-angle X-ray scattering (GIWAXS), and atomic force microscopy (AFM). These measurements show that the microstructural order (aggregation or crystallinity) remains largely intact after the applied strain. The polarization-sensitive devices displayed comparable performance characteristics to the control spun-cast devices, showing only a small reduction in responsivity and increase in dark current. The polarized devices also showed improved detection speed and noise equivalent power (NEP) compared to the spun-cast device. The obtained photodetector performance metrics are comparable to current state-of-the-art all-polymer organic detectors with the added polarization sensing capability. These results underscore the advantages that all-polymer photovoltaics have in achieving high-performance intrinsically polarization sensitivity photodetectors with broad spectral tunability.

2. Results and Discussion

The panchromatic absorption characteristics of the photodetectors are due to the complimentary absorption of PBnDT-FTAZ and P(NDI2OD-T2), as shown in Figure 2a. PBnDT-FTAZ primarily absorbs from 450 to 600 nm, while P(NDI2OD-T2) absorbs light below 450 nm and from 600 to 800 nm. Combined, the photodetector was sensitive from 350 to 800 nm. In addition to the complimentary absorption, the two polymers also have highest occupied molecular orbital (HOMO) and lowest unoccupied molecular orbital (LUMO) energy offsets that suggest efficient exciton dissociation, with values provided in Figure 1b.^[31,41] Despite the polymer blend using a 1:1 ratio by mass, it was found that the PBnDT-FTAZ absorption was much greater than the P(NDI2OD-T2), as depicted in Figure 2a. This is consistent with previous measurements that show a higher absorption coefficient of PBnDT-FTAZ compared with P(NDI2OD-T2).^[39,42]

Both polymers are ductile at room temperature, and when mixed, the resulting blend film largely maintains the ductility of the individual polymers.^[43] This enabled the blend films to be heavily strained while maintaining film continuity needed for functional devices. The large applied strain reoriented the polymer chains in the plane of the film inducing dichroism

across the absorption spectrum. This was quantified by considering the ratio of absorbance of light polarized parallel to the strain direction to the absorbance of light polarized perpendicular to the strain direction, referred to as the dichroic ratio. The dichroic ratio was found to increase with applied strain, as depicted in Figure 2b,c. It was found that the dichroic ratio is similar across the absorbance spectrum, suggesting both PBnDT-FTAZ and P(NDI2OD-T2) orient similarly with applied strain. The absorbance spectra of the films with various applied strain is provided in Figure S1 in the Supporting Information. The dichroic ratio for the films that underwent the largest applied strain of 60% was found to be above 1.7 from 500 to 900 nm. Tearing in the films was observed when strained beyond 65% and thus 60% strain was the limiting case considered in this study. While the applied strain was limited to 60%, the induced optical anisotropy covers a range targeted for polarimetry.^[15]

Along with the absorbance anisotropy, GIWAXS measurements of the films show clear orientation of the polymer crystals/aggregates. The images, given in Figure 3, show diffraction features from PBnDT-FTAZ and P(NDI2OD-T2). PBnDT-FTAZ is largely amorphous resulting in broad features at 1.65 and 0.32 \AA^{-1} associated with (010) and (100) planes. The P(NDI2OD-T2) is semicrystalline and multiple peaks are found in the GIWAXS images. In the unstrained films, there are in-plane (200) peaks associated P(NDI2OD-T2) that suggest that crystallites of this polymer pack primarily face-on.^[44,45] When strain oriented, GIWAXS measurements were made with the X-ray beam parallel and perpendicular to the strain direction. A clear anisotropy in diffraction was found in both polymers. The diffraction of the (100) and (010) peaks in PBnDT-FTAZ show crystallite realignment in the direction of applied strain. The P(NDI2OD-T2) is also found to align with the (00l) diffraction peaks being much stronger for the scattering vector nominally parallel to the strain direction. This is consistent with backbone alignment in the direction of strain. In-plane line scans from the 2D GIWAXS images are given in Figure S2 in the Supporting Information, clearly showing the packing anisotropy in the oriented films.

In addition to the orientation of the polymers in the blend, both the UV-vis and GIWAXS provide insight into the local order of the polymers. While PBnDT-FTAZ is largely

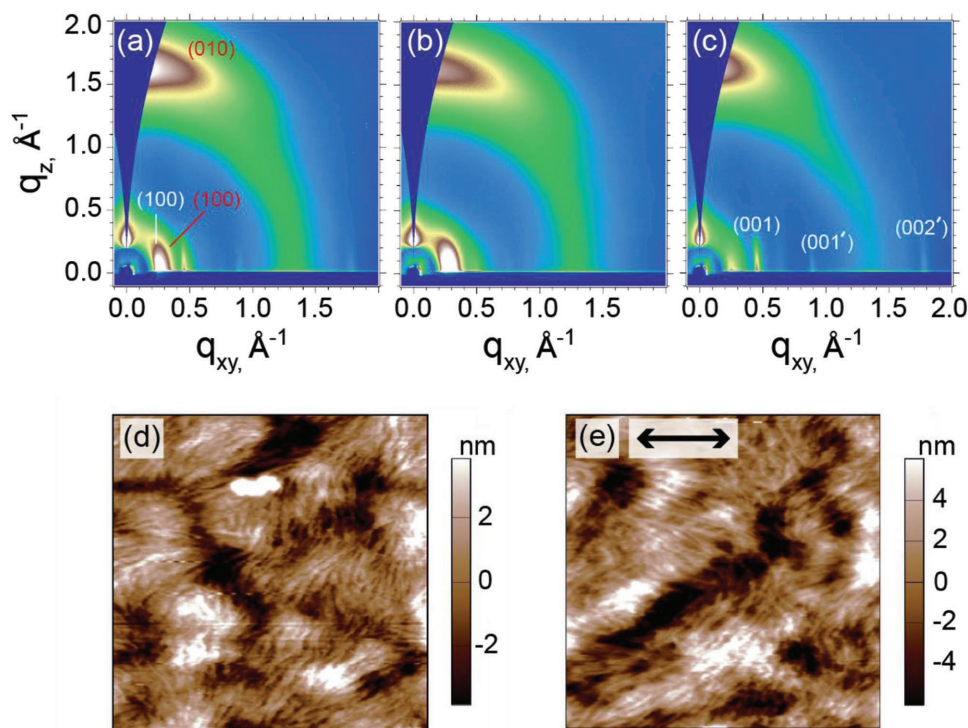


Figure 3. 2D GIWAXS images of PBnDT-FTAZ:P(NDI2OD-T2) films that were a) spun cast and b,c) uniaxially strained by 60%. In the strain-oriented film, the X-ray beam was incident nominally parallel (b) and perpendicular (c) to the applied strain direction. The scattering peaks are given for PBnDT-FTAZ in red, and P(NDI2OD-T2) in white. d) AFM height images of a spun-cast blend film on an ZnO/ITO substrate, and 60% strain aligned blend film that was initially cast on a PEDOT:PSS surface, strained and printed onto the ZnO/ITO surface. The arrow provided in e) indicates the applied strain direction. Both images are $1\ \mu\text{m} \times 1\ \mu\text{m}$.

amorphous, a vibronic progression in the absorbance was observed with peaks at 490, 535, and 576 nm. As depicted in Figure 2a, the three vibronic features found in the spun-cast film remain similar when strained. This is more clearly seen in the absorbance with polarized light parallel to the strain direction due to the alignment of the polymer aggregates. This suggests that PBnDT-FTAZ in the strain-oriented film retains similar local order to that in the spun-cast film. In contrast to PBnDT-FTAZ, P(NDI2OD-T2) does not have strong vibronic features in the absorbance spectra; however, there are clear GIWAXS diffraction peaks associated with its semicrystalline nature. In this case, the (00*l*) peaks observed in the spun-cast film remain in the strained films. In the indexed peaks in Figure 3(c) the (00*l*) and (00*l*') represent polymorphs.^[45] The alignment of the backbone makes these features much stronger when the diffraction is from the X-ray beam perpendicular to the strain direction. While determining a change in crystallinity is not possible without further mapping of the reciprocal space, the increased clarity of diffraction of the (00*l*) peaks suggest that the local order of P(NDI2OD-T2) was maintained after the application of strain. These results are consistent with previous measurements of strain-oriented neat polymer semiconductor and polymer-blend films.^[11,46] Finally, the film morphology of an unstrained films and 60% strained film was probed by AFM, with images given in Figure 3d,e. The films are observed to have a fibrillary microstructure that is maintained with applied strain. The films are also observed to be continuous with no signs of film fracture. While not definitive, there is

an appearance that the fibrils are orienting in the direction of applied strain.

The blend films were applied in photodetectors using an inverted device architecture, with details provided in the Experimental Section. The devices were optimized with emphasis on polarization sensitivity and responsivity. The all-polymer BHJ layer was made relatively thin (90–110 nm) to ensure polarization sensitivity across the absorption spectrum. If the active layer were designed to maximize responsivity and minimize dark current, they would have been made thicker. However, thicker films would have significant absorption of polarized light perpendicular to the polymer chain alignment direction, effectively reducing the polarization sensitivity. On the other hand, making the active layer thinner would maximize polarization sensitivity but would come at a cost of reduced responsivity and a likely increase in noise current, and thus negatively impact the sensor's detectivity. Holding the active layer to ≈ 100 nm lead to a good balance between responsivity and polarization sensitive.

The spectral response and polarization sensitivity was quantified by determining the responsivity (*R*) and external quantum efficiency (EQE) under linear polarized light. These two metrics and their relationship are given as

$$R = \frac{J_{\text{ph}}}{P_{\text{in}}} = \text{EQE} \frac{q}{h\nu} \quad (1)$$

where J_{ph} is the photocurrent, h is the Planck constant, ν is the light frequency, P_{in} is the light intensity, and q is electron charge.

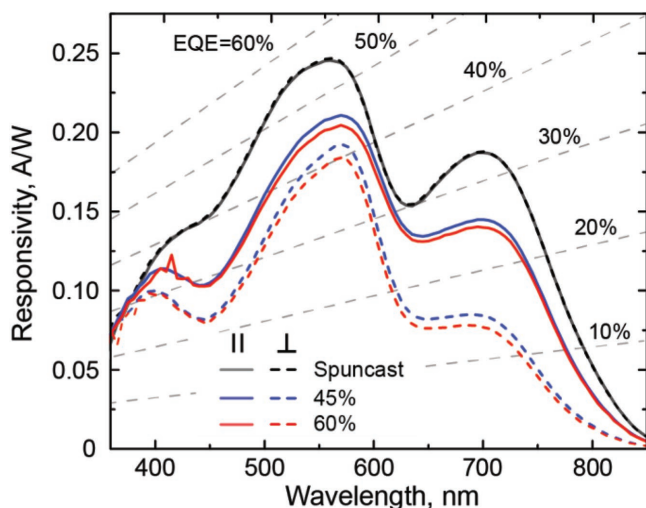


Figure 4. The responsivity of the detectors under a -0.5 V bias as a function of wavelength for spun-cast and 45% and 60% strain with contour lines depicting the corresponding biased EQE. The detectors are tested under linear polarized light parallel (||) and perpendicular (\perp) to the strain direction.

R and EQE of both the control spun-cast devices and strain-oriented devices under linearly polarized light parallel and perpendicular to the alignment direction is given in **Figure 4**, and Figure S3 in the Supporting Information. These tests were done under a -0.5 V bias, and thus the reported EQE is a biased EQE.^[16] The maximum R for a spun-cast device was 0.247 A W^{-1} at 560 nm. This is a significant increase over the current state-of-the-art all-polymer photodiodes that exhibited R of less than 0.15 A W^{-1} under -1 V bias.^[35,37] As expected, the spun cast-based devices had no polarization sensitivity. In the strain-oriented devices, R is given for films strained by 45% and 60%. Both films show clear photocurrent anisotropy with higher R when incident light is polarized parallel to the polymer alignment direction compared with the transverse polarized light. In addition to the induced anisotropy, there is also a decrease in the responsivity compared with the unpolarized devices. This is primarily attributed to a reduction in light absorption in the active layer due to a reduction in film thickness when being strain oriented. This reduced absorption is magnified when considering polarized light perpendicular to the chain alignment direction further reducing responsivity. There may be other losses associated with increased charge recombination in the strain-oriented device that may contribute to the lower responsivity that would require further analysis. However, previous analysis on strain-oriented P3HT:PCBM devices showed that internal quantum efficiency only slightly reduced compared to control spun-cast films, suggesting that the primary difference in EQE was due to absorption differences.^[47] Despite the reduced R (and EQE) in strain-oriented films, the performance metrics still compare favorably to other high-performing all-polymer photodetector demonstrations.

The current–voltage characteristics in the dark and under linear polarized white light illumination are provided in **Figure 5**. The strain-oriented devices show clear polarization sensitivity under illumination. This is highlighted by plotting the ratio of photocurrent for incident light parallel and light perpendicular to the polymer alignment direction, given

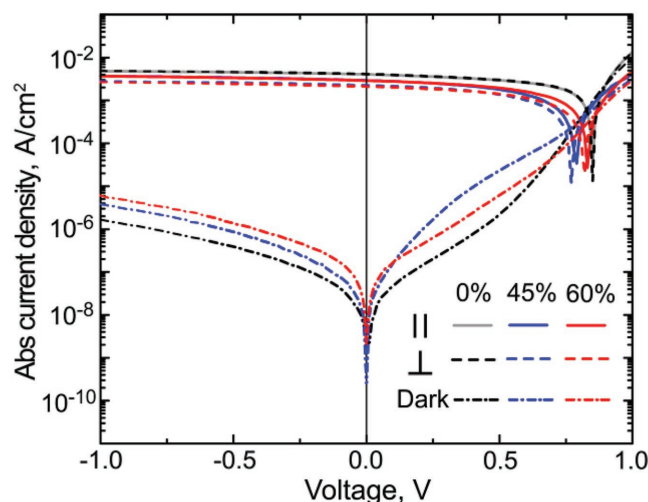


Figure 5. Current–voltage curves of spun-cast and strain-oriented detectors in the dark and under linear polarized illumination parallel (||) and perpendicular (\perp) to the direction of applied strain, with a white light intensity of 41 mW cm^{-2} .

in **Figure 2c**. The photocurrent ratio is found to increase with the amount of strain applied to the films and tracks closely with the measured dichroic ratio. The photocurrent anisotropy of 1.38 for the 60% strained film is comparable to previously demonstrated strain-oriented P3HT:PCBM devices despite having a lower peak dichroic ratio.^[14] This is attributed to the broadband polarization sensitivity of the PBnDT-FTAZ:P(NDI2OD-T2) device compared with the P3HT:PCBM based device where only the P3HT is polarization sensitive. The dark currents of the strain-oriented films are observed to be higher than the spun-cast control device. The dark current is also observed to increase with increasing amount of strain applied to the films.

We speculate that the strain process may result in an increase in trap states that result in charge hopping pathways that increase dark current. The larger leakage currents (lower shunt resistance) may also be associated with a decrease in film thickness with applied strain, and a possible increase in film roughness.^[48,49] This may be improved by using thicker active layers. However, it is important to note that the devices have been optimized for polarization sensitivity as opposed to detectivity. As mentioned above, increasing the film thickness will reduce polarization sensitivity. While larger dark current was found in the strain-oriented films, optimization of device interfaces will likely improve these results.^[50–52]

Having established that the devices show strong polarization sensitivity across a broad spectral range, it is important that the key photodetector performance metrics including detection sensitivity, linear dynamic range, and speed are determined.^[5,49] The detector sensitivity is characterized by the minimal detectable signal, which is represented by the NEP. The NEP represents the incident power that would be required to yield near-unity signal-to-noise ratio (SNR) over a bandwidth (B) of 1 Hz and is given by^[5,53]

$$\text{NEP} = \frac{i_n \sqrt{B}}{R} \quad (2)$$

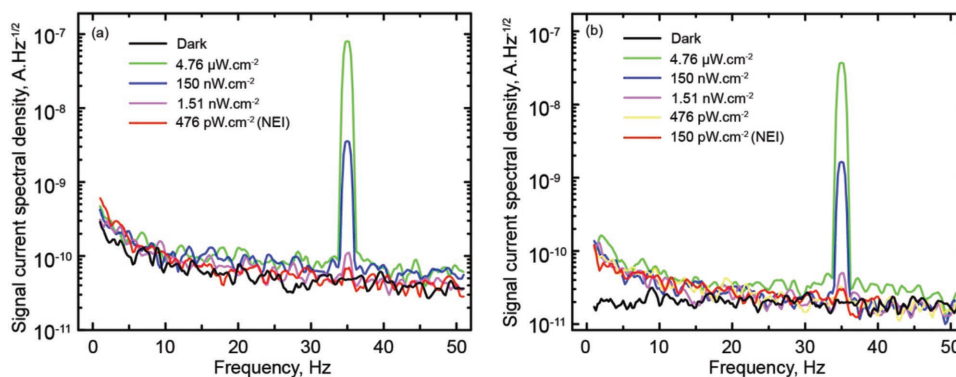


Figure 6. Signal current spectral densities of devices under 390 nm light being modulated at 35 Hz at different light intensity values, for a) a spun-cast detector, and b) a 45% strain-oriented detector. The detectors were measured under a -0.5 V bias.

where i_n is the noise current. The inverse of NEP normalized to the square root of device area (A) is the specific detectivity (D^*) given by

$$D^* = \frac{\sqrt{A}}{\text{NEP}} \quad (3)$$

The specific detectivity is typically the metric reported in the literature to describe the sensitivity of a photodetector.^[5,54] The detectivity is often determined by measuring or estimating the noise current and using the noise current along with responsivity. An alternative approach is to directly obtain the NEP by measuring the current spectral density under modulated light at various light intensities when the spectrum analyzer resolution bandwidth is set to 1 Hz. The point where the peak signal from the device under illumination cannot be distinguished from the noise current is then the noise equivalent irradiance (NEI), which can be converted to NEP.^[53] This approach was used to determine the NEP of the spun-cast and 45% strain devices, with measurements provided in **Figure 6**.

Despite having a thinner photoactive layer, the polarization-sensitive detector exhibited a lower NEI of 150 pW cm^{-2} compared to 476 pW cm^{-2} for a spun-cast detector. Considering an active device working area of 6.9 mm^2 , the NEPs for the corresponding strain-oriented and spun-cast detectors are 1.04×10^{-11} and $3.28 \times 10^{-11} \text{ W Hz}^{-1/2}$, respectively. These NEPs result in specific detectivities of 2.55×10^{10} and $0.8 \times 10^{10} \text{ cm Hz}^{1/2} \text{ W}^{-1}$. While there have been demonstrations of higher detectivity organic photodetectors, they have largely been achieved by lowering the noise current in the devices through charge-blocking layers or making thick active layers.^[49,50] The noise currents reported here should be able to be lowered through further optimization of the active layer interfaces. The NEP was also measured using a 390 nm light source, which corresponds to a spectral region of low responsivity. The specific detectivity should increase when the illumination wavelength corresponds with higher responsivity.

In the literature, a common assumption used to obtain D^* is to assume that the shot (dark) noise is the major contributor of noise in the system.^[6] While this allows for a straightforward calculation, it has been pointed out that this assumption can lead to a significant overestimation of the detectivity.^[49,53] The specific detectivities of the reported devices

using this assumption are given in **Figure S4** in the Supporting Information, showing values over $10^{11} \text{ cm Hz}^{1/2} \text{ W}^{-1}$ across the visible spectrum. These results show that this approach does indeed overestimate the detectivity of the photodetectors significantly. While erroneous, this method allows for a comparison to other detectors reported in the literature that use this method. Under this view, the performance of the polarized detectors compare well to other all-polymer organic photodetectors,^[34–38] and other intrinsic polarized detectors.^[54]

In addition to sensitivity, the temporal and linear dynamic range were also measured. Here, a 45% strain-oriented detector was compared to a spun-cast device. The dynamic range of the detectors is provided in **Figure 7a** demonstrates similar performance, with the strain-oriented device showing linearity down to $7.6 \times 10^{-6} \text{ A cm}^{-2}$. The linearity is found to approach the device's dark currents. The speed of the detectors were considered by measuring the -3 dB bandwidth, with frequency response plots for a spun-cast and 45% strain-oriented film given in **Figure 7b**. Interestingly, the strain-oriented device had a slightly higher 3 dB frequency cutoff and the response was found to drop more slowly at lower frequencies. The devices had 3 dB frequency cutoffs similar to other organic detectors at similar bias.^[55] The cutoff frequency should improve by using smaller active areas and increasing the negative bias applied to the devices.^[49] These changes will lower the effective capacitance of the device reducing the RC time constant and increase the speed of the detector.^[49] The important point here is that the spun-cast and polarization-sensitivity devices have similar performance in both linear dynamic range and speed.

It is worth comparing the performance of the all-polymer polarized detectors with other approaches and recent demonstrations. To start, the most common commercial photodiodes are based on silicon, which is not intrinsically polarization sensitive and require a polarizer to be integrated in front of the device to achieve the same functionality as the polarization-sensitive PBnDT-FTAZ:P(NDI2OD-T2) detectors. The addition of a wire-grid polarizer yields a reduction in photons that would be incident on the silicon detector due to the transmission loss by the polarizer. This is particularly true at lower wavelength values. Consider an FD11A silicon detector (Thorlabs), which has a responsivity of 0.168 A W^{-1} at 400 nm. If a broadband wire grid polarizer with a transmittance of 70% at 400 nm is placed in front of the device (e.g., WP12L-UB,

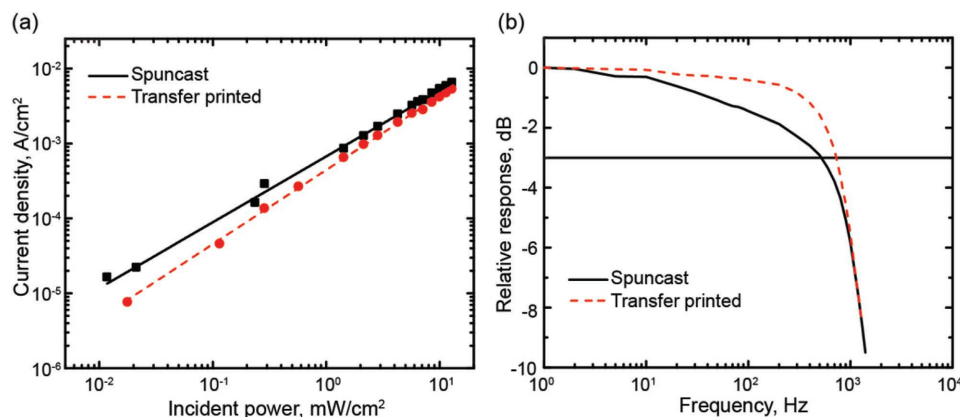


Figure 7. a) Current density of a spun-cast and 45% strain-oriented detector under -0.5 V bias as a function of incident light intensity provided by a 532 nm diode laser. b) Frequency response for the photodetectors measured under -0.1 V bias.

Thorlabs), the electrical output would be anticipated to be similar to the reported PBnDT-FTAZ:P(NDI2OD-T2) polarized detector that has a responsivity of 0.112 A W^{-1} . To remove the need for a polarizing optics in front of the detector, there have been recent reports that focus on exploiting the anisotropic properties of 2D materials for intrinsic sensitive photodetectors, such as TiS₃, black phosphorous, and others.^[54,56–60] The performance of the all-polymer photodetector reported here outperforms these demonstrations in terms of the combination of detectivity and response time. Although it should be noted that this is based on detectivities calculated assuming shot noise dominates the noise current, which was used in the other reports. There has also been a recent report of a polarization-sensitive perovskite photodetector.^[61] However, the detectivity was not provided to be able to compare performance.

3. Conclusion

We report a polarization-sensitive organic photodetector that is polarization sensitive across the visible spectrum. This was realized with an all-polymer active layer that has several advantages over other organic- and inorganic-based devices. First, the films are highly ductile so that the polarization sensitivity can be tuned through strain orienting a BHJ film composed of both polymers. The ductility also suggests that these devices would perform well in flexible device applications. A second key advantage is that the polymers employed have complimentary absorption and aligning both polymers with applied strain results in polarization sensitivity across the visible spectrum. This intrinsic polarization sensitivity removes the need for polarizers placed on the input side of a conventional detector, simplifying polarized light detectors. The performance of the detectors was thoroughly characterized showing that the polarization sensitivity is primarily due to the optical anisotropy of the active layer. While the polymers align in the direction of strain, the local polymer order in the film is kept allowing the films to maintain high quantum efficiency. In fact, the photodetector performance in terms of R , detectivity, and 3 dB cutoff frequency is among the highest reported for all-polymer photodetectors,^[35,37] and intrinsically polarization-sensitive organic or inorganic

photodetectors.^[15–17,54,56–60] In summary, the demonstrated devices highlight the opportunity of all-polymer photodetectors to achieve high-performance intrinsically polarization-sensitive photodetectors with broad spectral response.

4. Experimental Section

Device Fabrication: The fabrication process began with spin casting a poly(3,4 ethylenedioxythiophene):poly(styrenesulfonate) (PEDOT:PSS, Clevis 4083) film onto a donor glass substrate at 5000 rpm for 60 s.^[62] The films were then annealed in ambient air at 120 °C for 20 min. A PBnDT-FTAZ:P(NDI2OD-T2) blend was dissolved in chlorobenzene in a 1:1 mass ratio with a total concentration of 12 mg mL^{-1} and held at 90 °C overnight. The P(NDI2OD-T2) was obtained from Ossila and the PBnDT-FTAZ was synthesized using previously described methods.^[39] The solution was then cast warm onto the PEDOT:PSS coated glass substrate at 2000 rpm for 60 s. The thickness of the films was ≈ 110 nm as measured by variable angle spectroscopic ellipsometry. The glass substrate is laminated onto a polydimethylsiloxane (PDMS) slab that was attached to a custom-made mechanical strain stage. PDMS (Sylgard 184) was prepared at a 15:1 base to cross-linking ratio and cured in a vacuum oven for 12 h held at 85 kPa and 60 °C. The PDMS was ≈ 1 mm thick. The stage was then immersed in water to dissolve the underlying PEDOT:PSS layer leaving the PBnDT-FTAZ:P(NDI2OD-T2) film on the PDMS slab. A uniaxial strain is then applied to the film–elastomer composite. The aligned polymer films were then transferred to a partially fabricated detector that consisted of a ZnO film on an indium tin oxide (ITO)-coated glass. The transfer process used a previously described shear-assisted transfer printing (SHARP) technique.^[63] For spun-cast devices, the PBnDT-FTAZ:P(NDI2OD-T2) solution was directly spun cast on the ZnO/ITO glass. The ITO-coated glass was purchased from the South China Science & Technology Company Limited, and the ZnO deposition followed a previously detailed method.^[64] To complete the fabrication of the inverted architecture device, a 10 nm MoO₃ hole transport layer and 100 nm Al anode were deposited in a vacuum thermal evaporator at a pressure of $\approx 1 \times 10^{-6}$ mbar. The active area for the fabricated devices was 0.069 cm^2 .

Film Characterization: UV–vis optical absorption spectroscopy measurements were made with an Ocean Optics Jazz spectrometer. GIWAXS measurements were performed at the Stanford Synchrotron Radiation Lightsource (SSRL) on beamline 11-3 with an X-ray energy of 12.735 keV, and an incidence angle of $\approx 0.12^\circ$ with the samples in a helium enclosure. The scattering was recorded on a MAR CCD225 detector. The instrument was calibrated using a LaB₆ crystal standard. The AFM images were obtained using an Asylum MFP-3D-BIO.

Device Characterization: EQE and responsivity of the devices were measured using a DC xenon arc lamp light source, ORIEL 74125 monochromator, SR570 current amplifier, and SR830 DSP lock-in amplifier. The current–voltage characteristics of the devices were probed using a HP4156B semiconductor parameter analyzer. NEP was directly measured by a fast Fourier transform (FFT) signal analyzer (Agilent 35670A) which was connected to a low noise current preamplifier. A 35 Hz modulated LED with average emission wavelength of 390 nm was illuminated on the device. Light intensity was tuned and measured by a neutral density filter and optical power meter. These measurements were performed under a -0.5 V bias. Linearity measurements were taken using a 532 nm diode laser (Thorlabs DJ532-40) with intensity varied using neutral density filters. The frequency response of the devices was measured using a 410 nm LED light source modulated by a function generator. Linearity and frequency measurements were taken at a -0.5 and -0.1 V bias, respectively.

Supporting Information

Supporting Information is available from the Wiley Online Library or from the author.

Acknowledgements

This research was supported by the National Science Foundation award No 1407885 and award 1639429. Research by J. Huang and Y. Feng was supported by National Science Foundation award 1608610 and Department of Home Security under award 2014-DN-077-ARI069-05. The X-ray diffraction measurements were carried out at the Stanford Synchrotron Radiation Lightsource, a national user facility operated by Stanford University on behalf of the U.S. Department of Energy, Office of Basic Energy Sciences. The authors thank Prof. Harald Ade of NC State University for access to the group's thermal evaporator and photovoltaic testing station.

Conflict of Interest

The authors declare no conflict of interest.

Keywords

all-polymer, panchromatic, photovoltaic, polarimeter, polarized-light

Received: October 3, 2018
Revised: November 21, 2018
Published online:

- [1] J. Bailey, W. B. Sparks, J. H. Hough, D. J. Axon, *Nature* **1986**, 22, 1986.
- [2] F. Snik, J. Craven-Jones, M. Escuti, S. Fineschi, D. Harrington, A. De Martino, D. Mawet, J. Riedi, J. S. Tyo, presented at *Proc. SPIE - Int. Soc. Opt. Eng.*, Baltimore, MD, May **2014**.
- [3] M. Piels, J. E. Bowers, *Photodetectors: Materials, Devices and Applications* (Ed. B. Nabet), Elsevier, London, UK **2016**, pp. 3–20, <https://doi.org/10.1016/B978-1-78242-445-1.00001-4>.
- [4] K. Baeg, M. Binda, D. Natali, M. Caironi, Y. Noh, *Adv. Mater.* **2013**, 25, 4267.
- [5] F. P. Garcia de Arquer, A. Armin, P. Meredith, E. H. Sargent, *Nat. Rev.* **2017**, 2, 16100.
- [6] X. Gong, M. Tong, Y. Xia, W. Cai, J. S. Moon, Y. Cao, G. Yu, C.-L. Shieh, B. Nilsson, A. J. Heeger, *Science* **2009**, 325, 1665.
- [7] L. Xiao, S. Chen, X. Chen, X. Peng, Y. Cao, X. Zhu, *J. Mater. Chem. C* **2018**, 6, 3341.
- [8] B. M. Grell, D. D. C. Bradley, *Adv. Mater.* **1999**, 11, 895.
- [9] K. S. Whitehead, M. Grell, D. D. C. Bradley, M. Jandke, P. Stroehriegel, *Appl. Phys. Lett.* **2000**, 76, 2946.
- [10] M. C. Gather, D. D. C. Bradley, *Adv. Funct. Mater.* **2007**, 17, 479.
- [11] B. O'Connor, R. J. Kline, B. R. Conrad, L. J. Richter, D. Gundlach, M. F. Toney, D. M. DeLongchamp, *Adv. Funct. Mater.* **2011**, 21, 3697.
- [12] H. Tanaka, T. Yasuda, K. Fujita, T. Tsutsui, *Adv. Mater.* **2006**, 18, 2230.
- [13] R. Zhu, A. Kumar, Y. Yang, *Adv. Mater.* **2011**, 23, 4193.
- [14] O. Awartani, M. W. Kudenov, B. T. O'Connor, *Appl. Phys. Lett.* **2014**, 104, 093306.
- [15] S. Gupta Roy, O. M. Awartani, P. Sen, B. T. O'Connor, M. W. Kudenov, *Opt. Express* **2016**, 24, 14737.
- [16] R. Yang, P. Sen, B. T. O'Connor, M. W. Kudenov, *Appl. Opt.* **2017**, 56, 1768.
- [17] B. Döring, A. Sánchez-Díaz, A. Veciana, O. Arteaga, M. I. Alonso, M. Campoy-Quiles, *Adv. Opt. Mater.* **2017**, 5, 1700276.
- [18] M. S. Vezie, S. Few, I. Meager, G. Pieridou, B. Döring, R. S. Ashraf, A. R. Goñi, H. Bronstein, I. McCulloch, S. C. Hayes, M. Campoy-Quiles, J. Nelson, *Nat. Mater.* **2016**, 15, 746.
- [19] D. M. DeLongchamp, R. J. Kline, Y. Jung, D. S. Germack, E. K. Lin, A. J. Moad, L. J. Richter, M. F. Toney, M. Heaney, I. McCulloch, *ACS Nano* **2009**, 3, 780.
- [20] H. Tseng, L. Ying, B. B. Y. Hsu, L. A. Perez, C. J. Takacs, G. C. Bazan, A. J. Heeger, *Nano Lett.* **2012**, 12, 6353.
- [21] M. Brinkmann, J. Wittmann, *Adv. Mater.* **2006**, 18, 860.
- [22] B. G. Lussem, R. Festag, A. Greiner, C. Schmidt, C. Unterlechner, W. Heitz, J. H. Wendorf, M. Hopmeier, J. Feldmann, *Adv. Mater.* **1995**, 7, 923.
- [23] N. S. Sariciftci, U. Lemmer, D. Vacar, A. J. Heeger, R. A. J. Janssen, *Adv. Mater.* **1996**, 8, 651.
- [24] W. Chen, Q. Zhang, *J. Mater. Chem. C* **2017**, 5, 1275.
- [25] J. Zhang, H. S. Tan, X. Guo, A. Facchetti, H. Yan, *Nat. Energy* **2018**, 3, 720.
- [26] J. Hou, O. Inganäs, R. H. Friend, F. Gao, *Nat. Mater.* **2018**, 17, 119.
- [27] O. Awartani, B. I. Lemanski, H. W. Ro, L. J. Richter, D. M. De Longchamp, B. T. O'Connor, *Adv. Energy Mater.* **2013**, 3, 399.
- [28] J. Kim, I. Lee, T. Kim, N. Rolston, B. L. Watson, R. H. Dauskardt, *MRS Bull.* **2017**, 42, 115.
- [29] N. Balar, B. T. O'Connor, *Macromolecules* **2017**, 50, 8611.
- [30] T. Kim, J. Kim, T. E. Kang, C. Lee, H. Kang, M. Shin, C. Wang, B. Ma, U. Jeong, T. Kim, B. J. Kim, *Nat. Commun.* **2015**, 6, 8547.
- [31] L. Gao, Z. G. Zhang, L. Xue, J. Min, J. Zhang, Z. Wei, Y. Li, *Adv. Mater.* **2016**, 28, 1884.
- [32] X. Xu, Z. Li, W. Zhang, X. Meng, X. Zou, D. Di, C. Rasi, W. Ma, A. Yartsev, M. R. Andersson, R. A. J. Janssen, E. Wang, *Adv. Energy Mater.* **2018**, 8, 1700908.
- [33] X. Zhou, D. Yang, D. Ma, *Adv. Opt. Mater.* **2015**, 3, 1570.
- [34] J. Qi, W. Qiao, X. Zhou, D. Yang, J. Zhang, D. Ma, Z. Y. Wang, *Macromol. Chem. Phys.* **2016**, 217, 1683.
- [35] X. Wang, L. Lv, L. Li, Y. Chen, K. Zhang, H. Chen, H. Dong, J. Huang, G. Shen, Z. Yang, H. Huang, *Adv. Funct. Mater.* **2016**, 26, 6306.
- [36] L. Hu, W. Qiao, X. Zhou, X. Zhang, D. Ma, *Polymer* **2017**, 114, 173.
- [37] P. Murto, Z. Genene, C. M. Benavides, X. Xu, A. Sharma, X. Pan, O. Schmidt, C. J. Brabec, M. R. Andersson, S. F. Tedde, W. Mammo, E. Wang, *ACS Macro Lett.* **2018**, 7, 395.
- [38] X. Xu, X. Zhou, K. Zhou, Y. Xia, W. Ma, O. Inganäs, *Adv. Funct. Mater.* **2018**, 28, 1805570.
- [39] S. C. Price, A. C. Stuart, L. Yang, H. Zhou, W. You, *J. Am. Chem. Soc.* **2011**, 133, 4625.

- [40] H. Yan, Z. Chen, Y. Zheng, C. Newman, J. R. Quinn, F. Dötz, M. Kastler, A. Facchetti, *Nature* **2009**, 457, 679.
- [41] D. H. Wang, P. Morin, C. Lee, A. Ko, K. Kyaw, M. Leclerc, A. J. Heeger, *J. Mater. Chem. A* **2014**, 2, 15052.
- [42] Z. Li, W. Zhang, X. Xu, Z. Genene, D. Di Carlo Rasi, W. Mammo, A. Yartsev, M. R. Andersson, R. A. J. Janssen, E. Wang, *Adv. Energy Mater.* **2017**, 7, 1602722.
- [43] N. Balar, J. J. Rech, R. Henry, L. Ye, M. Ghasemi, R. J. Kline, H. Ade, W. You, B. T. O'Connor, in preparation.
- [44] W. Porzio, G. Scavia, L. Barba, G. Arrighetti, C. R. McNeill, *Eur. Polym. J.* **2014**, 61, 172.
- [45] M. Brinkmann, E. Gonthier, S. Bogen, K. Tremel, S. Ludwigs, M. Hufnagel, M. Sommer, *ACS Nano* **2012**, 6, 10319.
- [46] J. I. Scott, X. Xue, M. Wang, R. J. Kline, B. C. Hoffman, D. Dougherty, C. Zhou, G. Bazan, B. T. O'Connor, *ACS Appl. Mater. Interfaces* **2016**, 8, 14037.
- [47] O. Awartani, M. W. Kudenov, R. J. Kline, B. T. O'Connor, *Adv. Funct. Mater.* **2015**, 25, 1296.
- [48] A. Pierre, I. Deckman, P. B. Lechene, A. C. Arias, *Adv. Mater.* **2015**, 27, 6411.
- [49] A. Armin, M. Hamsch, I. K. Kim, P. L. Burn, P. Meredith, E. B. Namdas, *Laser Photonics Rev.* **2014**, 8, 924.
- [50] S. Xiong, L. Li, F. Qin, L. Mao, B. Luo, Y. Jiang, Z. Li, J. Huang, Y. Zhou, *ACS Appl. Mater. Interfaces* **2017**, 9, 9176.
- [51] X. Liu, J. Zhou, J. Zheng, M. L. Becker, X. Gong, *Nanoscale* **2013**, 5, 12474.
- [52] A. Grimoldi, L. Colella, L. La Monaca, G. Azzellino, M. Caironi, C. Bertarelli, D. Natali, M. Sampietro, *Org. Electron.* **2016**, 36, 29.
- [53] L. Shen, Y. Lin, C. Bao, Y. Bai, Y. Deng, M. Wang, T. Li, Y. Lu, A. Gruverman, W. Li, J. Huang, *Mater. Horiz.* **2017**, 4, 242.
- [54] Y. Niu, R. Frisenda, E. Flores, J. R. Ares, W. Jiao, D. P. de Lara, C. Sánchez, R. Wang, I. J. Ferrer, A. Castellanos-Gomez, *Adv. Opt. Mater.* **6**, **2018**, 1800351.
- [55] I. Deckman, P. B. Lechène, A. Pierre, A. C. Arias, *Org. Electron.* **2018**, 56, 139.
- [56] T. Hong, B. Chamlagain, W. Lin, H. Chuang, M. Pan, Z. Zhou, Y.-Q. Xu, *Nanoscale* **2014**, 6, 8978.
- [57] T. Hong, B. Chamlagain, T. Wang, H. Chuang, Z. Zhou, Y. Xu, *Nanoscale* **2015**, 7, 18537.
- [58] H. Yuan, X. Liu, F. Afshinmanesh, W. Li, G. Xu, J. Sun, B. Lian, A. G. Curto, G. Ye, Y. Hikita, Z. Shen, S. Zhang, X. Chen, M. Brongersma, H. Y. Hwang, Y. Cui, *Nat. Nanotechnol.* **2015**, 10, 707.
- [59] L. Ye, P. Wang, W. Luo, F. Gong, L. Liao, T. Liu, L. Tong, J. Zang, J. Xu, W. Hu, *Nano Energy* **2017**, 37, 53.
- [60] F. Liu, S. Zheng, X. He, A. Chaturvedi, J. He, W. L. Chow, T. R. Mion, X. Wang, J. Zhou, Q. Fu, H. J. Fan, B. K. Tay, L. Song, R. H. He, C. Kloc, P. M. Ajayan, Z. Liu, *Adv. Funct. Mater.* **2016**, 26, 1169.
- [61] J. Feng, X. Yan, Y. Liu, H. Gao, Y. Wu, B. Su, L. Jiang, *Adv. Mater.* **2017**, 29, 1605993.
- [62] Certain commercial equipment, or materials are identified in this paper in order to specify the experimental procedure adequately. Such identification is not intended to imply recommendation or endorsement by the National Institute of Standards and Technology, nor is it intended to imply that the materials or equipment identified are necessarily the best available for the purpose.
- [63] P. Sen, Y. Xiong, Q. Zhang, S. Park, W. You, H. Ade, M. W. Kudenov, B. T. O'Connor, *ACS Appl. Mater. Interfaces* **2018**, 10, 31560.
- [64] Y. Sun, J. H. Seo, C. J. Takacs, J. Seifert, A. J. Heeger, *Adv. Mater.* **2011**, 23, 1679.